HHS Public Access

Author manuscript

Nat Genet. Author manuscript; available in PMC 2015 March 11.

Published in final edited form as:

Nat Genet. 2014 February ; 46(2): 194–199. doi:10.1038/ng.2858.

Antagonistic roles of ubiquitin ligase HEI10 and SUMO ligase RNF212 regulate meiotic recombination

Huanyu Qiao[1,2], **H.B.D. Prasada Rao**[1,2], **Ye Yang**[1,2], **Jared H. Fong**[1,2], **Jeffrey M. Cloutier**[3], **Dekker C. Deacon**[3], **Kathryn E. Nagel**[3], **Rebecca K. Swartz**[3], **Edward Strong**[4], **J. Kim Holloway**[5], **Paula E. Cohen**[5], **John Schimenti**[4], **Jeremy Ward**[3], and **Neil Hunter**[1,2,6,7]

[1]Howard Hughes Medical Institute, University of California, Davis, Davis, California, USA

[2]Department of Microbiology & Molecular Genetics, University of California, Davis, Davis, California, USA

[3]Department of Biology, Middlebury College, Middlebury, Vermont, USA

[4]Department of Molecular Biology & Genetics, Cornell University College of Veterinary Medicine, Ithaca, New York USA

[5]Center for Reproductive Genomics, Department of Biomedical Sciences, Cornell University, Ithaca, New York, USA

[6]Department of Molecular & Cellular Biology, University of California, Davis, Davis, California, USA

[7]Department of Cell Biology & Human Anatomy, University of California, Davis, Davis, California, USA

Abstract

Crossover recombination facilitates accurate segregation of homologous chromosomes during meiosis[1,2]. In mammals, poorly characterized regulatory processes ensure every pair of chromosomes obtains at least one crossover, even though the majority of recombination sites yield non-crossovers[3]. Designation of crossovers involves selective localization of SUMO-ligase RNF212 to a minority of recombination sites where it stabilizes pertinent factors, such as MutSγ[4]. Here we show ubiquitin-ligase HEI10/CCNB1IP1[5,6] is essential for this crossover/non-crossover differentiation process. In *Hei10* mutant mice, RNF212 localizes to most recombination sites and dissociation of RNF212 and MutSγ from chromosomes is blocked. Consequently, recombination is impeded and crossing-over fails. In wild-type mice, HEI10 accumulates at designated crossover sites suggesting a late role to implement crossing-over. Like RNF212, dosage-sensitivity indicates

Correspondence should be addressed to N.H. (nhunter@ucdavis.edu).

AUTHOR CONTRIBUTIONS

H.Q., H.B.D.P.R., Y.Y., J.W. and N.H. conceived and designed the experiments. H.Q., H.B.D.P.R., Y.Y., J.H.F. J.C., D.D, K.N., R.S., E.S, J.K.H., J.W. and N.H. performed the experiments. H.Q., H.B.D.P.R., Y.Y., J.H.F., J.W. and N.H. analyzed the data. J.S., E.S. and P.E.C. contributed reagents, materials and/or analysis tools. H.Q., H.B.D.P.R., Y.Y., J.W. and N.H. wrote the manuscript.

COMPETING FINANCIAL INTERESTS

The authors declare no competing financial interests.

HEI10 is a limiting factor for crossing-over. We suggest SUMO and ubiquitin play antagonistic roles during meiotic recombination that are balanced to effect differential stabilization of recombination factors at crossover and non-crossover sites.

Variants of both *RNF212* and *HEI10/CCNB1IP1* are associated with heritable variation in the rate of crossing-over in humans[7–10]. Rnf212 and Hei10 also share structural and functional similarities. Both proteins have tripartite structures with RING, coiled-coil and tail domains, and are inferred to catalyze post-translational protein modification by ubiquitin-like proteins[4–6,11,12]. Rnf212 is implicated as an E3 enzyme for SUMO modification while Hei10 has ubiquitin-ligase activity[4,5,11](Y.Y and N.H, unpublished observations). In both *Hei10*$^{mei4/mei4}$ and *Rnf212*$^{-/-}$ mutant mice, early stages of meiosis occur normally and full synapsis of homologous chromosomes (homologs) is achieved[4,6]. However, crossover-specific recombination complexes, containing the MutLγ complex (MLH1 and MLH3) and cyclin-dependent kinase CDK2, fail to assemble[4,6]. Consequently, crossing-over fails and the animals are sterile. These similarities prompted us to examine the relationship between these two pro-crossover factors.

Using immunofluorescence cytology, we previously described the dynamic localization pattern of RNF212 to synaptonemal complexes[4], the meiosis-specific structures that connect homologous chromosomes (homologs) along their lengths during the pachytene stage of meiosis. As homologs undergo synapsis during zygonema, RNF212 localizes specifically to the central region of synaptonemal complexes forming a punctate pattern of immuno-staining foci. Consistent with previous analysis[4], in wild-type spermatocytes at early pachynema, when synapsis is complete, ~150 foci are observed per nucleus (Fig. 1a,k). However, by mid-pachynema, most staining has disappeared and RNF212 foci are retained only at sites where crossovers will form (Fig. 1b,c,k). These crossover-specific RNF212 foci are then lost by late pachynema, prior to the disassembly of synaptonemal complexes at diplonema (Fig. 1d,e,k).

In spermatocytes from *Hei10*$^{mei4/mei4}$ mice, the early staining pattern of abundant RNF212 foci appears normal (155.9 ± 37.2 (s.d.), 20 early pachytene nuclei; versus 153.0 ± 42.8 in wild type, 20 nuclei; Fig. 1f,k). Strikingly, this pattern persists throughout pachynema and loss of RNF212 from the chromosomes is only seen when synaptonemal complexes are disassembled during diplonema (Fig. g,h,i,j,k). Moreover, the numbers of RNF212 foci are significantly higher than ever seen in wild-type spermatocytes (P = 0.0003, Mann-Whitney test). Thus, HEI10 is required for the post-synapsis turnover of RNF212 that culminates in its selective retention at future crossover sites.

To examine the consequences of persistent RNF212 for recombination in *Hei10*$^{mei4/mei4}$ mutants, we examined chromosomal dynamics of the MutSγ complex (Fig. 2). MutSγ comprises MSH4 and MSH5, two meiosis-specific homologs of the bacterial DNA mismatch-binding factor MutS[13]. Evidence to date indicates that MutSγ binds and stabilizes DNA strand-exchange intermediates to promote both homolog synapsis and crossing-over[14,15]. We previously showed that a minority of MutSγ foci present in early pachynema co-localizes with RNF212[4]. Analysis of *Rnf212*$^{-/-}$ knock-out mice indicates that RNF212

acts to stabilize MutSγ and thereby designate a crossover fate to this subset of recombination sites.

In wild-type spermatocytes, chromosomal localization of MutSγ resembles that of RNF212: 82.9 ± 23.4 (s.d.) MSH4 immunostaining foci are observed in late zygonema and early pachynema; at mid pachynema only 39.4 ± 9.6 foci are retained; and by the onset of diplonema, MSH4 staining has essentially disappeared (Fig. 2a–e,k). In *Hei10*$^{mei4/mei4}$ mutant spermatocytes, chromosomal dynamics of MutSγ are severely aberrant. Although normal numbers of MSH4 foci are formed, focus numbers remain high throughout pachynema and only decrease after homologs desynapse at diplonema (Fig. 2f–k).

Super-resolution structured illumination microscopy (SIM[16]) reveals that stabilization of MutSγ foci correlates with the degree of co-localization between MutSγ and RNF212 (Fig. 2l–p and Supplementary Fig. 1). Consistent with our previous analysis[4], around a third of MSH4 foci colocalize with RNF212 in late zygotene and early pachytene spermatocytes (Fig. 2l,m,p; Supplementary Fig. 1). In sharp contrast, in *Hei10*$^{mei4/mei4}$ mutant spermatocytes, MSH4 foci show a high level of colocalization (~90%) with RNF212 at all stages from early zygonema through early diplonema (Fig. 2l–p; Supplementary Fig. 1). These observations lend further support to our inference that RNF212 stabilizes association of MutSγ with recombination sites[4]. Thus, RNF212 and HEI10 have antagonistic functions with respect to the stabilization of MutSγ at recombination sites. We suggest that the balance of these two activities underpins the temporal dynamics and spatial patterning of RNF212 and MutSγ seen in wild-type spermatocytes.

Meiotic recombination is initiated by the programed formation of DNA double-strand breaks (DSBs[15]). The persistence of MutSγ complexes implies that DSB-repair is delayed in *Hei10*$^{mei4/mei4}$ spermatocytes. Immunostaining for DSB-induced H2AX phosphorylation (γH2AX) supports this inference (Fig. 3). In wild-type nuclei, γH2AX staining initially forms a pan-nuclear cloud, which diminishes to limited chromatin flares and foci as chromosome synapsis ensues, and finally disappears from autosomes around mid pachynema[17] (Fig. 3a–e,k; note that γH2AX accumulates as a large staining body on the chromatin of the sex chromosomes where it facilitates transcriptional silencing[18]). In *Hei10*$^{mei4/mei4}$ spermatocytes, although pan-nuclear γH2AX staining diminishes with synapsis, delayed DSB-repair is indicated by the persistence of γH2AX foci throughout pachynema (Fig. 3f–j,k). Ultimately, however, DSBs appear to be repaired in *Hei10*$^{mei4/mei4}$ spermatocytes because broken chromatids are not detected in late-stage nuclei[6]. Together, these data suggest that HEI10-dependent elimination of RNF212 from synaptonemal complexes is required for the timely removal of MutSγ from most recombination sites as pachynema progresses. This in turn allows the timely progression of recombination and repair of DSBs.

Despite their broadly similar phenotypes, we can now conclude that *Rnf212*$^{-/-}$ and *Hei10*$^{mei4/mei4}$ mutants have distinct defects with respect to the designation of crossover sites. In the absence of RNF212, designation of crossover sites fails because no MutSγ complexes are stabilized beyond early pachynema[4]; whereas absence of HEI10 causes most

or all MutSγ complexes to be stabilized, as though all sites have been designated a crossover fate. This raises the question, why don't *Hei10*$^{mei4/mei4}$ mutants form lots of crossovers?

Insights into this question, and how HEI10 regulates the dynamics of RNF212 and MutSγ, came from examining the chromosomal localization patterns of HEI10. Although previous attempts to localize mouse HEI10 to meiotic chromosomes failed[6], we were able to show that mouse HEI10 associates with synaptonemal complexes to form distinct immunostaining foci (Fig. 4a–k and Supplementary Figs. 2 and 3). Unlike RNF212, distinct foci of HEI10 were rarely detected along nascent synaptonemal complexes during zygonema (Fig. 4a). Given that *Hei10*$^{mei4/mei4}$ phenotypes are already apparent at this time (e.g. Fig. 2p), we infer that cytologically undetectable HEI10 regulates early-stage dynamics of RNF212 and MutSγ. Indeed, the possibility this function of HEI10 does not involve association with meiotic chromosomes cannot be ruled out. However, by early pachynema, HEI10 foci could be detected (Fig. 4c,d) and their numbers peaked during mid pachynema with an average of 27 foci per nucleus (27.2 ± 8.8 (s.d.); 22 nuclei; Fig. 4e,f,k). At this stage, HEI10 focus numbers were quite variable, with as few as 15 and as many as 50 foci per nucleus. In late pachytene nuclei, the average HEI10 focus number was lower and less variable (21.1 ± 3.6 (s.d.); 20 nuclei; Fig. 4g,h,k). At the onset of diplonema, HEI10 foci were no longer detected (Fig. 4i,j).

As HEI10 promotes loss of RNF212 and MutSγ from synaptonemal complexes, we examined co-localization with these proteins (Fig. 4l–o). In mid-pachytene spermatocytes, only 23% of RNF212 foci and 29% of MSH4 foci colocalized with HEI10 (respectively, 22.6 ± 7.7% (s.d.) and 28.9 ± 15.1%, 10 nuclei each). HEI10 is required for formation of crossover-specific complexes containing CDK2 and MutLγ (MLH1-MLH3). In contrast to RNF212 and MSH4, a high degree of co-localization was seen between these crossover-specific markers and HEI10 (Fig. 4p–s). 74.0 ± 10.7% (s.d.) of non-telomeric CDK2 foci and 94.3 ± 6.9% of MLH1 foci co-localized with HEI10 (10 and 19 nuclei respectively). These data are consistent with HEI10 foci superseding co-complexes of RNF212 and MutSγ at future crossover sites.

The genetic requirements for chromosomal localization of HEI10 were investigated using several mutant lines. SPO11 catalyzes DNA breakage to initiate recombination[15]. In *Spo11*$^{-/-}$ spermatocytes, homolog pairing is defective but a significant fraction of nuclei assemble incomplete synaptonemal complexes, which generally involve non-homologous chromosomes[19,20]. HEI10 foci were diminished, although not completely eliminated, in these nuclei (Fig. 5a,b,g). This dependency contrasts that of RNF212, which readily associates with synaptonemal complexes independently of recombination[4]. SYCP1 encodes a major component of the synaptonemal complex central region[21]. In the *Sycp1* knockout mice, meiotic recombination initiates normally and homologs closely coalign, but synapsis is precluded. Also, MutLγ foci are not detected in *Sycp1*$^{-/-}$ nuclei indicating that designation or maturation of crossover sites fails in this mutant. Formation of HEI10 foci was greatly reduced in pachytene-like *Sycp1*$^{-/-}$ spermatocytes, but most nuclei contained a few foci (4.5 ± 3.1 (s.d.) per nucleus, 20 nuclei; Fig. 5c,d,g). In *Rnf212*$^{-/-}$ mutants, homologs undergo synapsis but designation of crossover sites is defective[4]. Similar to the *Sycp1*$^{-/-}$ mutant, a few HEI10 foci were detected in *Rnf212*$^{-/-}$ mutant spermatocytes (6.7 ±

4.9 (s.d.), 23 nuclei; Fig. 5e,f,g). We infer that initiation of recombination, homolog synapsis and the designation of crossover sites are important for the normal formation and/or stabilization of HEI10 foci.

Finally, we examined HEI10 localization in mice lacking the MLH3 component of the crossover-specific factor, MutLγ[13]. In *Mlh3*$^{-/-}$ spermatocytes, homolog synapsis and initial designation of crossover sites appear normal, but implementation of crossing-over fails [4,22]. In sharp contrast to the other mutants examined, high numbers of HEI10 foci were observed in *Mlh3*$^{-/-}$ spermatocytes (Fig. 5h–m). Unlike wild-type, HEI10 foci were already detectable in zygonema (Fig. 5h,i,n), reached very high numbers during mid pachynema (89.9 ± 24.5 (s.d.) foci per nucleus, 21 nuclei; Fig. 4j,k,n) and persisted into diplonema (Fig. 5l,m,n). At least half of the foci in mid pachynema were coincident with γH2AX staining (53.0 ± 12.5% (s.d.), 10 nuclei; Supplementary Figure 4), implying that the majority of HEI10 accumulates at sites of DSB repair in *Mlh3*$^{-/-}$ cells.

These data suggest that chromosomal localization of HEI10 occurs in two phases: first, HEI10 is licensed to accumulate into foci associated with synaptonemal complexes. These, normally transient, complexes may generally promote progression of recombination. In wild type, the relatively high and variable numbers of HEI10 foci seen in mid pachynema may be a manifestation of this first phase. Subsequently, stable accumulation of HEI10 specifically at crossover sites is directed by MLH3 (and, presumably, MLH1). Notably, MLH3 restrains accumulation of HEI10 during zygonema, an early function that was not anticipated from the timing of crossover-specific MLH3 foci, which don't appear until early-mid pachynema[13].

Taken together, our data imply that HEI10 functions during zygonema to limit the co-localization of RNF212 with MutSγ-associated recombination sites and thereby establish early differentiation of crossover and non-crossover sites. Later, HEI10 is directed by MutLγ (and perhaps CDK2) to stably accumulate at designated crossover sites. Here, we propose that HEI10 also promotes dissociation of RNF212 and MutSγ to allow progression of recombination and implementation of the final steps of crossing over. CNTD1 is a cyclin-B related protein and the mammalian homolog of the *C. elegans* pro-crossover factor, COSA-1[23]. Intriguingly, the meiotic phenotypes of *Cntd1*$^{-/-}$ and *Hei10*$^{mei4/mei4}$ mice are remarkably similar and CNTD1 is required for chromosomal localization of HEI10, suggesting that the two proteins function together (P. Cohen, personal communication). The model in Supplementary Figure 5 synthesizes the key points of our analysis and those of previous studies.

Recently, recombination rate in humans has been associated with a variant in the untranslated 5′ region of *HEI10/CNNB1IP1* (A. Kong, personal communication), which has the potential to alter expression level and suggests that Hei10 may be a dosage-sensitive regulator of crossing over. To determine whether the crossover function of mouse HEI10 is dosage sensitive, we analyzed spermatocytes from *Hei10*$^{+/mei4}$ heterozygotes (Fig. 6). Indeed, significant decreases in the numbers HEI10 foci (20.6%), MLH1 foci (13.5%) and chiasmata (10%) were detected (P=0.0003, < 0.0001 and 0.0088, respectively; Mann-Whitney test). In spermatocytes, homologs not tethered by crossovers are detected by the

spindle checkpoint, which triggers apoptosis[24]. Consistent with the reduced crossing-over seen in *Hei10* $^{+/mei4}$ heterozygotes, we detected a significant increase in apoptotic cells (TUNEL positive) in testes sections from *Hei10*$^{+/mei4}$ heterozygotes (Fig. 6j–m and Supplementary Fig. 6; $P < 0.0001$ Mann-Whitney test).

Intriguingly, the crossover function of RNF212 also shows dosage sensitivity in the mouse, and human *Rnf212* variants have been associated with changes in recombination rate[4,7–9]. These observations are consistent with the idea that the balance of SUMO and ubiquitin is a key aspect of crossover regulation. It will be interesting to see if human alleles of *HEI10/CNNB1IP1, RNF212* and recombination factors such as MutSγ, interact to modulate recombination rate, fertility and the risk of aneuploidy.

ONLINE METHODS

Mice

All mice were congenic with the C57BL/6J background. Mice were maintained and used for experimentation according to the guidelines of the Institutional Animal Care and Use Committees of the University of California, Davis and the Middlebury College Animal Facility. The *Hei10*, *Mlh3*, *Rnf212*, *Spo11* and *Sycp1* mutant lines and primer sequences for genotyping were previously described[4,6,19,21,22]. Male mice between 2–6 months were used for experimentation.

Protein blot analysis

Tissues from adult mice were sonicated in RIPA buffer, protein concentration was measured by the Bradford assay and 100–200 μg of protein was separated by SDS-PAGE. After protein transfer to nitrocellulose membranes (Waterman), blots were incubated overnight with the following antibodies: mouse monoclonal anti-CCNB1IP1/HEI10 (ab118999 Abcam, 1:2000 dilution), rabbit polyclonal anti-CCNB1IP1/HEI10 (this study, 1:2000), or mouse anti-tubulin (BioLegend, 625902, 1:2,000). Secondary antibodies (1:10,000 dilution) were goat anti-rabbit or anti-mouse IgGs conjugated to horseradish peroxidase (HRP; SouthernBiotech, 4050-05 and 1031-05, respectively). HRP was detected using the ECL reagent (Pierce).

Antibody Production

A polyclonal antibody against mouse HEI10/CCNB1IP1 was raised in rabbits against a mixture of two C-terminal peptides. Antibodies were purified from serum using Protein A/G spin columns (GE Healthcare).

Cytology

Testes and ovaries were dissected from freshly killed animals and processed for surface spreading as described[25]. For all quantification, images from at least two animals (2–5) were analyzed. Comparisons were made between animals that were either littermates or matched by age. All cytological analyses were performed by two observers; the second observer was blind to which group/genotype was being analyzed. Immunofluorescence staining was performed as described[26], using the following primary antibodies with incubation overnight

at room temperature: mouse anti-SYCP3 (sc-74568 Santa Cruz, 1:200 dilution), rabbit anti-SYCP3 (sc-33195 Santa Cruz, 1:300), guinea pig anti-SYCE1[27] (1:2000)(generously provided by Chist Höög, Karolinska Institutet), guinea pig anti-RNF212[4] (1:50), rabbit anti-RNF212[4] (1:200), rabbit anti-MSH4 (ab58666 Abcam, 1:100), mouse monoclonal anti-CCNB1IP1/HEI10 (ab118999 Abcam, 1:150), rabbit polyclonal anti-CCNB1IP1/HEI10 (this study,), mouse anti-MLH1 (1:50, 550838 BD Pharmingen), mouse monoclonal anti-γH2AX (05-636 Millipore, 1:500), mouse monoclonal anti-CDK2 (sc-6248 Santa Cruz, 1:200), guinea pig anti-H1t[28] (a gift from M.A. Handel, The Jackson Laboratory; 1:1,000 dilution). Slides were subsequently incubated with the following goat secondary antibodies for 1 h at 37 °C: anti-rabbit 488 (A11070 Molecular Probes, 1:1000 dilution), anti-rabbit 568 (A11036 Molecular Probes, 1:2000), anti-mouse 555 (A21425 Molecular Probes, 1:1000), anti-mouse 594 (A11020 Molecular Probes, 1:1000), anti-mouse 488 (A11029 Molecular Probes, 1:1000), and anti-guinea pig fluorescein isothiocyanate (106-096-006 FITC, Jackson Labs, 1:200). Coverslips were mounted with ProLong Gold antifade reagent (Molecular Probes). For chiasma counts, air-dried preparations of diakinesis/metaphase I–stage cells were prepared as described[29] and stained with DAPI.

TUNEL Assay

Testes were fixed in formalin, embedded in paraffin, sectioned and processed using the ApopTag Plus Peroxidase In Situ Apoptosis Detection kit (Chemicon).

Imaging

Immunolabeled chromosome spreads and DAPI-stained diakinesis/metaphase I nuclei were imaged using a Zeiss AxioPlan II microscope with 63× Plan Apochromat 1.4 objective and EXFO X-Cite metal halide light source. Images were captured by a Hamamatsu ORCA-ER CCD camera and processed using Volocity (Perkin Elmer) and Photoshop (Adobe) software packages. SIM analysis was performed using a Nikon N-SIM super-resolution microscope system and NIS-Elements 2 image processing software. MSH4-RNF212 colocalization was determined using NIS-Elements and co-foci were confirmed by visual inspection. Testes sections were imaged using an Axiovert 200 microscope and AxioCamMRc camera using AxioVision 4.4 software. Apoptotic cells were imaged and counted in representative fields of view.

Supplementary Material

Refer to Web version on PubMed Central for supplementary material.

Acknowledgments

We thank A. Kong for communicating unpublished results. This work was supported by US National Institutes of Health (NIH) grant R01GM084955 to N.H., R01GM45415 to J.S. HD041012 to P.E.C. and a National Science Foundation grant CAREER 0844941 to J.W. N.H. is an Investigator of the Howard Hughes Medical Institute.

References

1. Sakuno T, Tanaka K, Hauf S, Watanabe Y. Repositioning of aurora B promoted by chiasmata ensures sister chromatid mono-orientation in meiosis I. Dev Cell. 2011; 21:534–45. [PubMed: 21920317]
2. Hirose Y, et al. Chiasmata promote monopolar attachment of sister chromatids and their co-segregation toward the proper pole during meiosis I. PLoS Genet. 2011; 7:e1001329. [PubMed: 21423721]
3. Jones GH. The control of chiasma distribution. Symp Soc Exp Biol. 1984; 38:293–320. [PubMed: 6545727]
4. Reynolds A, et al. RNF212 is a dosage-sensitive regulator of crossing-over during mammalian meiosis. Nat Genet. 2013; 45:269–78. [PubMed: 23396135]
5. Toby GG, Gherraby W, Coleman TR, Golemis EA. A novel RING finger protein, human enhancer of invasion 10, alters mitotic progression through regulation of cyclin B levels. Mol Cell Biol. 2003; 23:2109–22. [PubMed: 12612082]
6. Ward JO, et al. Mutation in mouse hei10, an e3 ubiquitin ligase, disrupts meiotic crossing over. PLoS Genet. 2007; 3:e139. [PubMed: 17784788]
7. Kong A, et al. Sequence variants in the RNF212 gene associate with genome-wide recombination rate. Science. 2008; 319:1398–401. [PubMed: 18239089]
8. Fledel-Alon A, et al. Variation in human recombination rates and its genetic determinants. PLoS ONE. 2011; 6:e20321. [PubMed: 21698098]
9. Chowdhury R, Bois PR, Feingold E, Sherman SL, Cheung VG. Genetic analysis of variation in human meiotic recombination. PLoS Genet. 2009; 5:e1000648. [PubMed: 19763160]
10. Kong, Aea. Common and low-frequency variants associated with genome-wide recombination rate. Nat Genet. 2013 in press.
11. Cheng CH, et al. SUMO modifications control assembly of synaptonemal complex and polycomplex in meiosis of Saccharomyces cerevisiae. Genes Dev. 2006; 20:2067–81. [PubMed: 16847351]
12. Strong ER, Schimenti JC. Evidence Implicating CCNB1IP1, a RING Domain-Containing Protein Required for Meiotic Crossing Over in Mice, as an E3 SUMO Ligase. Genes (Basel). 2010; 1:440–451. [PubMed: 21779533]
13. Kolas NK, Cohen PE. Novel and diverse functions of the DNA mismatch repair family in mammalian meiosis and recombination. Cytogenet Genome Res. 2004; 107:216–31. [PubMed: 15467367]
14. Snowden T, Acharya S, Butz C, Berardini M, Fishel R. hMSH4-hMSH5 recognizes Holliday Junctions and forms a meiosis-specific sliding clamp that embraces homologous chromosomes. Mol Cell. 2004; 15:437–51. [PubMed: 15304223]
15. Hunter, N. Meiotic Recombination. In: Aguilera, A.; Rothstein, R., editors. Molecular Genetics of Recombination. Springer-Verlag; Heidelberg: 2006. p. 381-442.
16. Carlton PM. Three-dimensional structured illumination microscopy and its application to chromosome structure. Chromosome Res. 2008; 16:351–65. [PubMed: 18461477]
17. Chicheportiche A, Bernardino-Sgherri J, de Massy B, Dutrillaux B. Characterization of Spo11-dependent and independent phospho-H2AX foci during meiotic prophase I in the male mouse. J Cell Sci. 2007; 120:1733–42. [PubMed: 17456548]
18. Fernandez-Capetillo O, et al. H2AX is required for chromatin remodeling and inactivation of sex chromosomes in male mouse meiosis. Dev Cell. 2003; 4:497–508. [PubMed: 12689589]
19. Baudat F, Manova K, Yuen JP, Jasin M, Keeney S. Chromosome synapsis defects and sexually dimorphic meiotic progression in mice lacking Spo11. Mol Cell. 2000; 6:989–98. [PubMed: 11106739]
20. Romanienko PJ, Camerini-Otero RD. The mouse Spo11 gene is required for meiotic chromosome synapsis. Mol Cell. 2000; 6:975–87. [PubMed: 11106738]
21. de Vries FA, et al. Mouse Sycp1 functions in synaptonemal complex assembly, meiotic recombination, and XY body formation. Genes Dev. 2005; 19:1376–89. [PubMed: 15937223]

22. Lipkin SM, et al. Meiotic arrest and aneuploidy in MLH3-deficient mice. Nat Genet. 2002; 31:385–90. [PubMed: 12091911]
23. Yokoo R, et al. COSA-1 reveals robust homeostasis and separable licensing and reinforcement steps governing meiotic crossovers. Cell. 2012; 149:75–87. [PubMed: 22464324]
24. Eaker S, Cobb J, Pyle A, Handel MA. Meiotic prophase abnormalities and metaphase cell death in MLH1-deficient mouse spermatocytes: insights into regulation of spermatogenic progress. Dev Biol. 2002; 249:85–95. [PubMed: 12217320]
25. Holloway JK, Booth J, Edelmann W, McGowan CH, Cohen PE. MUS81 generates a subset of MLH1-MLH3-independent crossovers in mammalian meiosis. PLoS Genet. 2008; 4:e1000186. [PubMed: 18787696]
26. Qiao H, Lohmiller L, Anderson L. Cohesin proteins load sequentially during prophase I in tomato primary microsporocytes. Chromosome Research. 2011; 19:193–207. [PubMed: 21234670]
27. Costa Y, et al. Two novel proteins recruited by synaptonemal complex protein 1 (SYCP1) are at the centre of meiosis. J Cell Sci. 2005; 118:2755–2762. [PubMed: 15944401]
28. Cobb J, Cargile B, Handel MA. Acquisition of competence to condense metaphase I chromosomes during spermatogenesis. Dev Biol. 1999; 205:49–64. [PubMed: 9882497]
29. Holloway JK, Morelli MA, Borst PL, Cohen PE. Mammalian BLM helicase is critical for integrating multiple pathways of meiotic recombination. J Cell Biol. 2010; 188:779–89. [PubMed: 20308424]

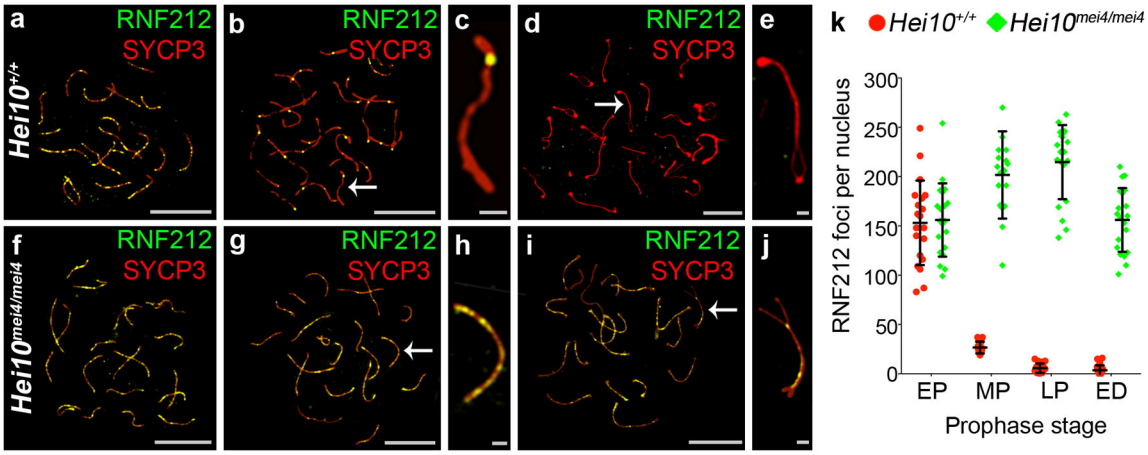

Figure 1.

RNF212 fails to dissociate from synaptonemal complexes in *Hei10* $^{mei4/mei4}$ mutant spermatocytes. All nuclei were immunostained for RNF212 (green) and homolog axis component, SYCP3 (red). (**a**–**e**) Wild-type (*Hei10* $^{+/+}$) nuclei at (**a**) early pachynema, (**b,c**) mid pachynema, and (**d,e**) early diplonema. **c** and **e** show magnified views of chromosomes indicates by arrows in **b** and **d**, respectively. (**f**–**j**) *Hei10* $^{mei4/mei4}$ mutant nuclei at (**f**) early pachynema, (**g,h**) midpachynema, and (**i,j**) early diplonema. **h** and **j** show magnified views of chromosomes indicated by arrows in **g** and **j**, respectively. (**k**) Quantification of RNF212 foci (± s.d.) at successive prophase I stages. EP, early pachynema; MP, mid pachynema; LP, late pachynema; ED, early diplonema. 20 nuclei were analyzed for each stage.

Scale bars, 10 μm in **a,b,d,f,g,i** and 1μm in **c,e,h,j**.

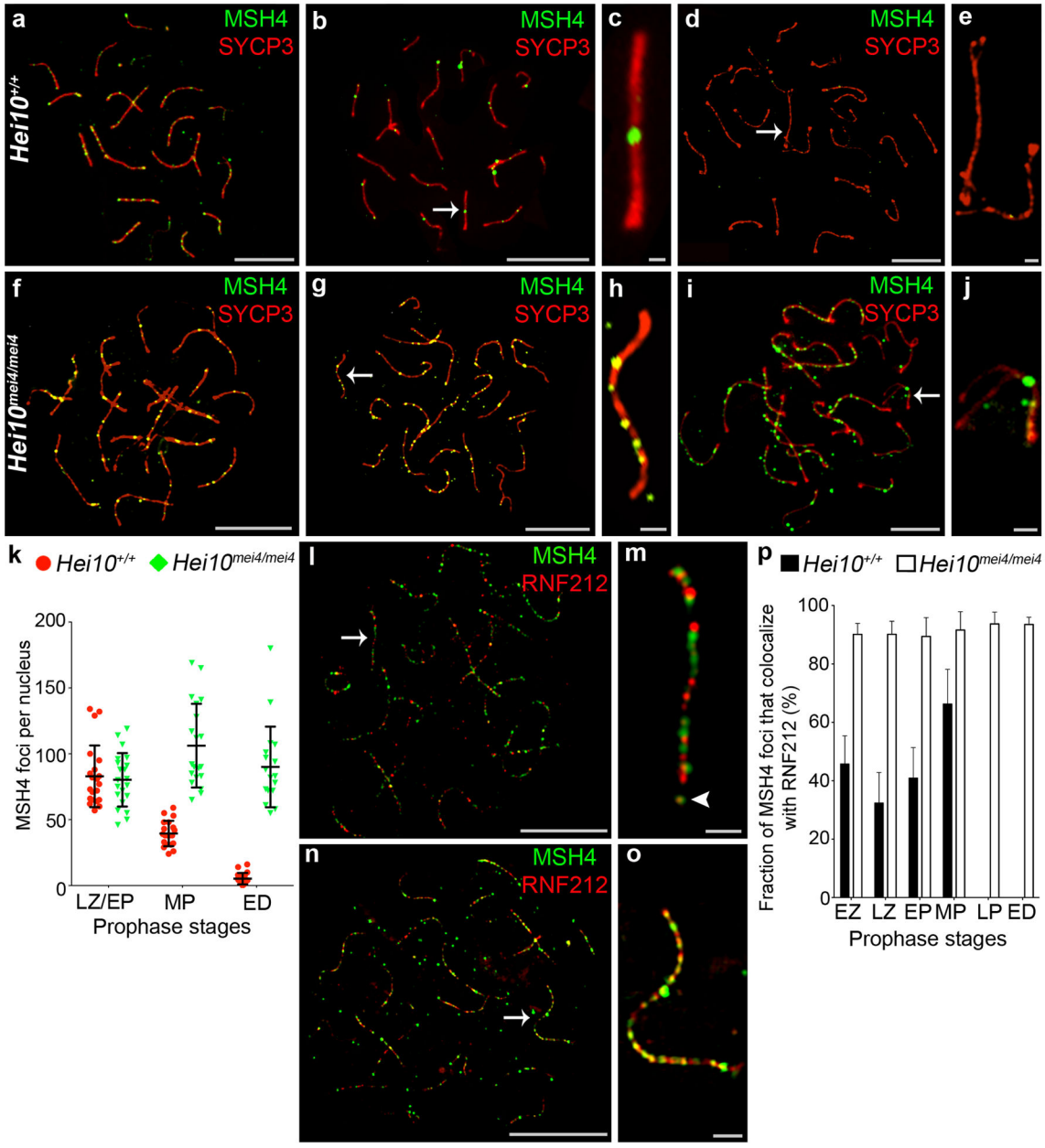

Figure 2.

Persistence of MutSγ complexes in *Hei10*$^{mei4/mei4}$ spermatocytes. (**a–j**) Spermatocyte nuclei immunostained for MSH4 (green) and SYCP3 (red). (**a–e**) Wild-type nuclei at (**a**) late zygonema, (**b,c**) mid pachynema, and (**d,e**) early diplonema. **c** and **e** show magnified views of chromosomes indicated by arrows in **b** and **d**, respectively. (**f–j**) *Hei10*$^{me4/mei4}$ mutant nuclei at (**f**) late zygonema, (**g,h**) mid pachynema, and (**i,j**) early diplonema. **h** and **j** show magnified views of chromosomes indicated by arrows in **g** and **j**, respectively. (**k**) Quantification of MSH4 foci (± s.d.) at successive prophase I stages. LZ, late zygonema; EP, early pachynema; ED, early diplonema. Number of nuclei analyzed at LZ/EP, MP and ED: 21, 20 and 20 for *Hei10* $^{+/+}$; and 21, 20 and 18 for *Hei10* $^{mei4/mei4}$. (**l–o**) SIM images of

early pachytene nuclei immunostained for MSH4 (red) and RNF212 (green). To allow accurate staging, nuclei were also stained for SYCP3 (not shown). (**l**) Wild-type nucleus. (**m**) Magnification of the chromosome highlighted by the arrow in **l**. (**n**) *Hei10*$^{me4/mei4}$ mutant nucleus. (**o**) Magnification of the chromosome highlighted by the arrow in **n**. (**p**) Percentage of MSH4 foci (± s.d.) that colocalize with RNF212 at successive prophase substages determined by SIM analysis. EZ, early zygonema; LZ, late zygonema; EP, early pachynema; MP, mid pachynema; LP, late pachynema; ED, early diplonema. Number of *Hei10*$^{+/+}$ nuclei analyzed at EZ, LZ, EP and MP, respectively: 10, 5, 10, and 7. Number of *Hei10*$^{mei4/mei4}$ nuclei analyzed at EZ, LZ, EP, MP, LP and ED, respectively 5, 6, 25, 14, 9, 9.

Scale bars, 10 μm in **a,b,d,f,g,i,l,n** and 1μm in **c,e,h,j,m,o**.

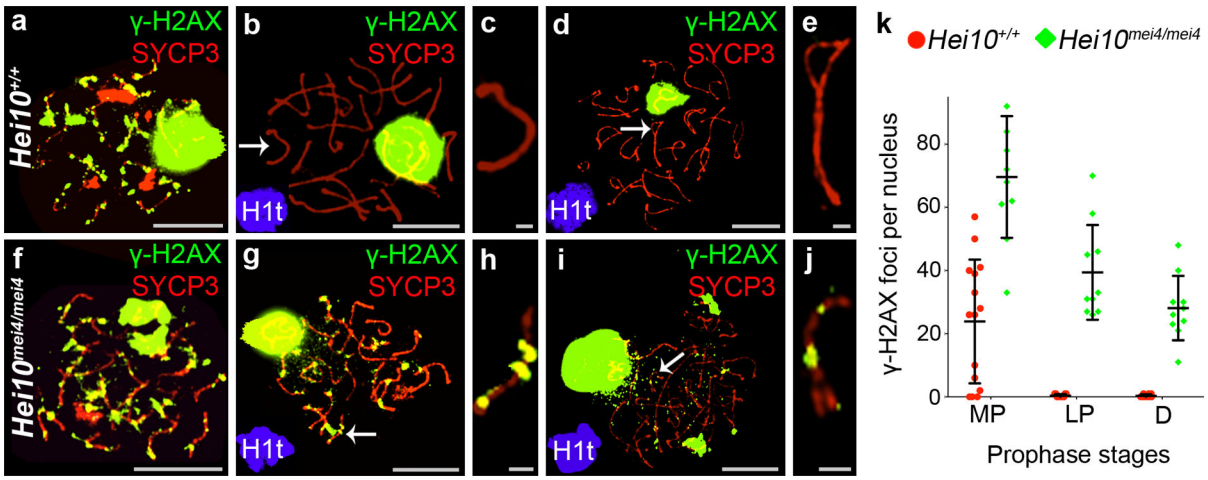

Figure 3.

Repair of DSBs is delayed in *Hei10*$^{mei4/mei4}$ spermatocytes. All nuclei were immunostained for γH2AX (green) and SYCP3 (red). (**a**–**e**) Wild-type nuclei at (**a**) early pachynema, (**b,c**) mid pachynema, and (**d,e**) diplonema. **c** and **e** show magnified views of chromosomes indicates by arrows in **b** and **d**, respectively. (**f**–**j**) *Hei10*$^{mei4/mei4}$ mutant nuclei at (**f**) early pachynema, (**g,h**) mid pachynema, and (**i,j**) early diplonema. **h** and **j** show magnified views of chromosomes indicates by arrows in **g** and **j**, respectively. (**k**) Quantification of γH2AX foci (± s.d.) at successive prophase I stages. MP, mid pachynema; LP, late pachynema; D, diplonema. Number of nuclei analyzed at MP, LP and D: 15, 11 and 10 for *Hei10* $^{+/+}$; and 10, 10 and 10 for *Hei10* $^{mei4/mei4}$.

Scale bars, 10 μm in **a,b,d,f,g,i** and 1μm in **c,e,h,j**.

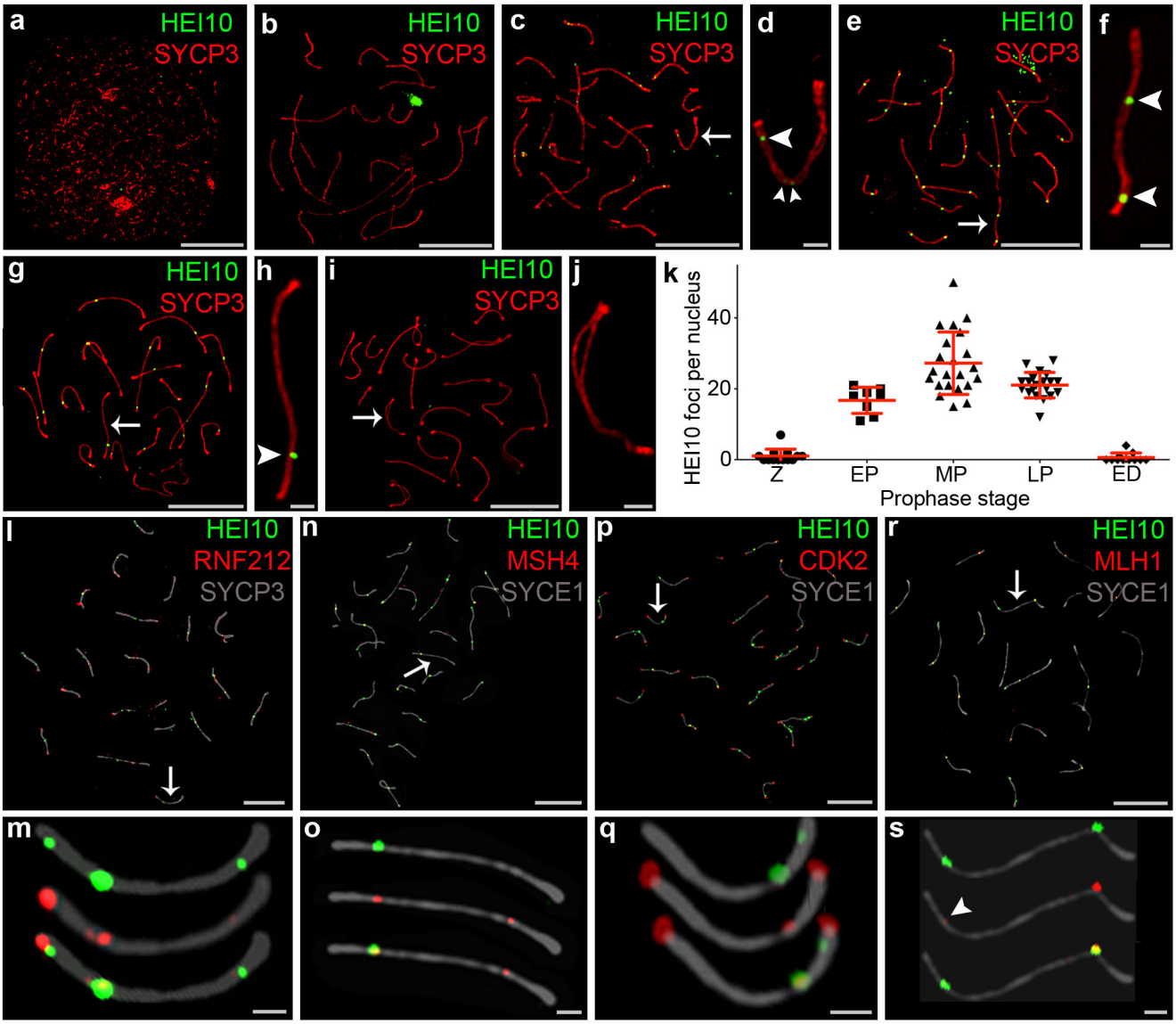

Figure 4.

HEI10 localization to synaptonemal complexes and crossover sites. (**a–j**) Representative SIM images of wild-type spermatocyte nuclei immunostained for HEI10 (green) and SYCP3 (red) at (**a**) leptonema, (**b**) late zygonema, (**c,d**) early pachynema, (**e,f**) mid pachynema, (**g,h**) late pachynema, and (**i,j**) early diplonema. (**d, f, h, j**) Magnified views of the chromosomes indicated by arrows in **c, e, g, i**, respectively. Arrowheads highlight HEI10 foci. (**k**) Numbers of HEI10 foci per nucleus at successive prophase stages (Z, zygonema; EP, early pachynema; MP, mid pachynema; LP, late pachynema; ED, early diplonema). Horizontal bars represent means ± s.d. Numbers of nuclei analyzed at Z, EP, MP, LP and ED, respectively: 13, 8, 22, 20 and 11. (**l,m**) Mid-pachytene spermatocyte immunostained for HEI10 (green), RNF212 (red), and SYCP3 (grey). (**m**) Magnified view of the chromosome indicated by the arrow in **l**. (**n,o**) Mid-pachytene spermatocyte immunostained for HEI10 (green), MSH4 (red) and synaptonemal complex central element protein, SYCE1

(grey). (**o**) Magnified view of the chromosome indicated by the arrow in **n**. (**p,q**) Mid-pachytene spermatocyte immunostained for HEI10 (green), CDK2 (red), and SYCE1 (grey). (**q**) Magnified view of the chromosome indicated by the arrow in **p**. (**r,s**) Mid-pachytene spermatocyte immunostained for HEI10 (green), MLH1 (red), and SYCE1 (grey). (**s**) Magnified view of the chromosome indicated by the arrow in **r**. The arrowhead highlights a small MLH1 focus that colocalizes with HEI10.

Scale bars, 10 μm in **a, b, c, e, g, i, l, n, p, r**; 1 μm in **d, f, h, j, m, o, q, s**.

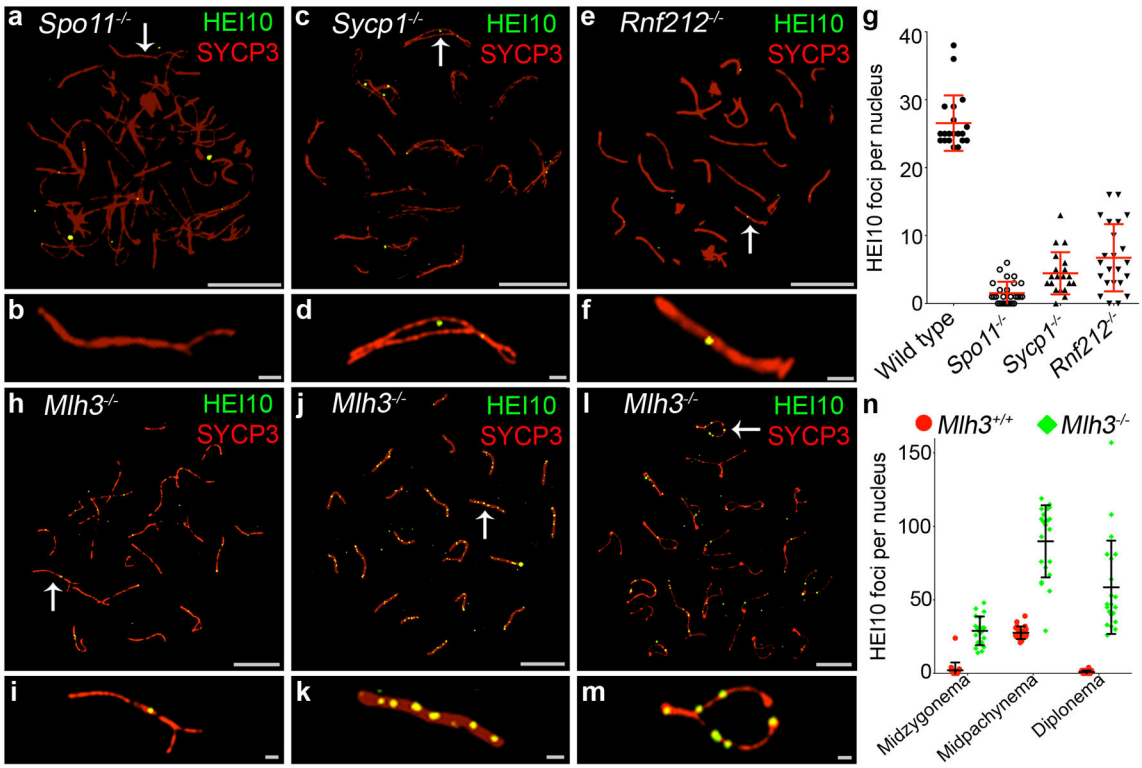

Figure 5.

Genetic requirements for HEI10 localization. (**a**–**m**) Representative spermatocyte nuclei, from indicated mutant lines, immunostained for HEI10 (green) and SYCP3 (red). (**a,b**) Spermatocyte nucleus from a *Spo11*$^{-/-}$ mouse. (**b**) Magnification of the chromosome indicated by the arrow in **a**. (**c,d**) Spermatocyte nucleus from a *Sycp1*$^{-/-}$ mouse. (**d**) Magnification of the chromosome indicated by the arrow in **c**. (**e,f**) Spermatocyte nucleus from a *Rnf212*$^{-/-}$ mouse. (**f**) Magnification of the chromosome indicated by the arrow in **e**. (**g**) Numbers of HEI10 foci per nucleus in mid-late pachytene spermatocytes from wild-type, *Spo11*$^{-/-}$, *Sycp1*$^{-/-}$ and *Rnf212*$^{-/-}$ mice. Bars represent means ± s.d. Numbers of nuclei analyzed: wild-type, 20; *Spo11*$^{-/-}$, 27; *Sycp1*$^{-/-}$, 20; *Rnf212*$^{-/-}$, 23. Analysis of *Spo11*$^{-/-}$ was confined to nuclei with high levels of synapsis, predicted to be the equivalents of mid pachynema nuclei. Similarly, only *Sycp1*$^{-/-}$ nuclei with a high degree of pseudo-synapsis were analyzed. However, true equivalents of wild-type mid pachynema nuclei may not be represented in *Spo11*$^{-/-}$ and *Sycp1*$^{-/-}$ testes due to apoptosis[18,20]. (**h**–**m**) Representative spermatocyte nuclei from the *Mlh3*$^{-/-}$ mutant. (**h**) Late zygotene nucleus. (**i**) Magnification of the chromosome indicated by the arrow in **h**. (**j**) Mid-pachytene nucleus. (**k**) Magnification of the chromosome indicated by the arrow in **j**. (**l**) Mid-diplotene nucleus. (**m**) Magnification of the chromosome indicated by the arrow in **m**. (**n**) Numbers of HEI10 foci per nucleus (± s.d.) at successive prophase stages in wild-type and *Mlh3*$^{-/-}$ mice. MZ, mid-zygonema; MP, mid pachynema; D, diplonema. Number of nuclei analyzed at MZ, MP and D, respectively: 20, 22 and 20 for wild-type (*Mlh3*$^{+/+}$); and 20, 21 and 21 for *Mlh3*$^{-/-}$. Scale bars, 10 μm in **a,c,e,h,j,l** and 1μm in **b,d,f,i,k,m**.

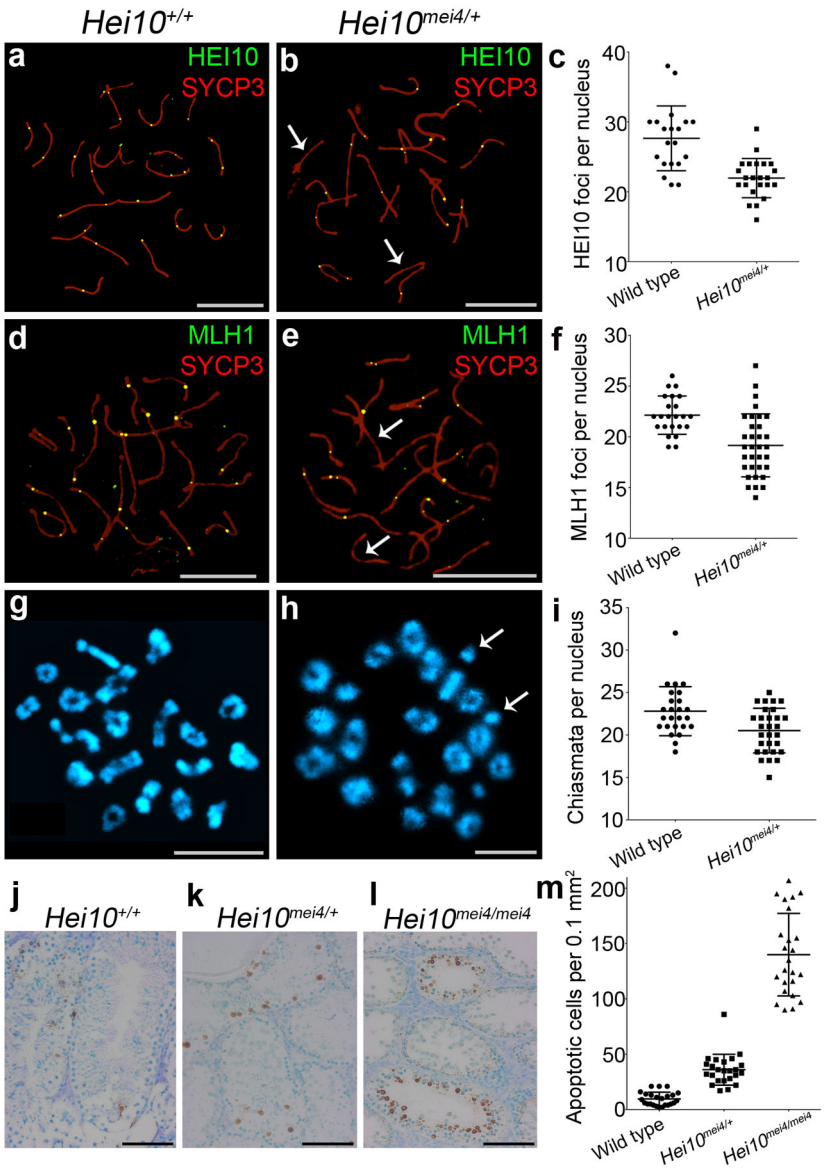

Figure 6.

Dosage sensitivity of the HEI10 crossover function. (**a,b**) Mid-pachytene nuclei from (**a**) wild-type (*Hei10*$^{+/+}$) and (**b**) *Hei10*$^{+/mei4}$ heterozygous mice immunostained for HEI10 (green) and SYCP3 (red). The arrows in **b** highlight chromosomes that lack HEI10 foci. (**c**) Numbers of HEI10 foci (± s.d.) per nucleus in mid-pachytene cells (23 wild-type and 33 *Hei10*$^{+/mei4}$ nuclei). (**d,e**) Mid-pachytene nuclei from (**d**) wild-type and (**e**) *Hei10*$^{+/mei4}$ heterozygous mice immunostained for MLH1 and SYCP3. The arrows in **e** highlight chromosomes that lack MLH1 foci. (**f**) Numbers of MLH1 foci per nucleus (± s.d.) in mid-pachytene cells (20 wild-type and 23 *Hei10*$^{+/mei4}$ nuclei). (**g, h**) Chromosome spreads of diakinesis/metaphase I spermatocytes from (**g**) wild-type and (**h**) *Hei10*$^{+/mei4}$ heterozygous mice stained with DAPI. (**i**) Numbers of chiasmata per nucleus (± s.d.) in diakinesis/metaphase I spermatocytes (25 wild-type and 29 *Hei10*$^{+/mei4}$ nuclei). (**j–l**) TUNEL stained

testis sections from (**j**) *Hei10*$^{+/+}$, (**k**) *Hei10*$^{+/mei4}$ and (**l**) *Hei10*^{mei4mei4} animals. (**m**) Quantification of TUNEL-positive apoptotic cells (± s.d.) in spermatocyte sections. Scale bars, 10 μm in **a,b,d,e,g,h** and 100 μm in **j,k,l**.